Valence-Shell Charge Concentrations and Electron Delocalization in Alkyllithium Complexes: Negative Hyperconjugation and Agostic Bonding

Wolfgang Scherer,*[a] Peter Sirsch,[a] Dmitry Shorokhov,[a] G. Sean McGrady,*[b] Sax A. Mason,[c] and Michael G. Gardiner[d]

Dedicated to Professor Gottfried Huttner on the occasion of his 65th birthday

Abstract: In this paper we present the results of density functional theory (DFT) calculations on the ethyl ligand and some related organic moieties; we then proceed to consider a range of alkyllithium complexes studied by DFT calculations and high-resolution X-ray and neutron diffraction. Topological analysis of the charge density is used to follow changes in the electronic structure of the organic fragment. The charge concentrations (CCs) in the valence shell at the α and β atoms reveal faithfully the delocalization of the lone pair at the C_α atom or of the Li–C bonding electrons. Negative hyperconjugation is thus shown to arise from delocalization of the lone pair or the Li–C bonding electrons over the alkyl fragment, with depletion of the metal-directed charge concentration at C_α, and characteristic ellipticity profiles for the bonds involved in hyperconjugative delocalization. In the case of so-called lithium agostic complexes, we show that close Li···H contacts are a consequence of this delocalization and further secondary interactions, with Li···H–C agostic interactions, playing only a minor role. The ellipticity profiles and the magnitude of the CCs at C_α provide a quantitative measure of the extent of delocalization, and show excellent agreement between experiment and theory.

Keywords: agostic interactions · alkyllithium complexes · charge density analysis · density functional calculations · lithium · negative hyperconjugation

Introduction

Electron delocalization and its concomitant stabilization is a natural feature of the molecular orbital approach to bonding.[1] In 1932 Pauling introduced the concept of resonance into the valence bond model to account for the stabilization observed in π-conjugated organic systems;[2, 3] Wheland and others subsequently developed these ideas further.[4] The concept of hyperconjugation was introduced by Mulliken at about the same time to account for the stabilization attendant on $\sigma \rightarrow \pi^*$ delocalization.[5] Somewhat later, the idea of negative (anionic) hyperconjugation was proposed by Roberts to include the effects of $\pi \rightarrow \sigma^*$ delocalization.[6] Negative hyperconjugation is often also referred to as the generalized anomeric effect.[7] In spite of long-standing controversy about its nature, negative hyperconjugation has been shown to have widespread and important energetic and geometrical consequences.[8]

Hyperconjugation has found much favor in the valence bond approach popular with organic chemists, being invoked to account for a variety of stereoelectronic effects in the structure and reactivity of organic compounds.[9] It has been demonstrated very recently that hyperconjugation, rather than steric repulsion, is the primary cause that determines molecular conformation in simple organic molecules like ethane.[10]

Although beautifully simple in concept, the effects of hyperconjugative delocalization have proved remarkably difficult to quantify in a general manner on the basis of

[a] Dr. W. Scherer, P. Sirsch, Dr. D. Shorokhov
Anorganisch-chemisches Institut
Technische Universität München
Lichtenbergstrasse 4, 85747 Garching bei München (Germany)
Fax: (+49) 89-289-13473
E-mail: wolfgang.scherer@ch.tum.de

[b] Dr. G. S. McGrady
Department of Chemistry, King's College London
Strand, WC2R 2LS (UK)

[c] Dr. S. A. Mason
Institut Laue-Langevin, BP156
38042 Grenoble cedex 9 (France)

[d] Dr. M. G. Gardiner
School of Chemistry, University of Tasmania
GPO Box 252-75, Hobart TAS 7001 (Australia)

Supporting Information for this article is available on the WWW under http://www.wiley-vch.de/home/chemistry or from the author. This includes: listing of geometrical and topological parameters of **8** and the calculated model systems; fractional atomic coordinates and mean square atomic displacement parameters of the neutron and X-ray studies; multipole population coefficients; expansion-contraction coefficients; description of the local coordinate system used in the multipolar refinements; model deformation and residual density maps and the comparison of multipole models with different flexibility.

  0947-6539/02/0810-2324 $ 20.00+.50/0

experimental observables. Whereas its geometrical consequences can be followed by careful structural studies, concomitant changes in electronic structure are rather difficult to trace by experiment. However, analysis of the topology of the charge density exploiting the "atoms in molecules" (AIM) approach[11] offers a powerful method with which to analyze the electronic effects of delocalization. Pioneering studies by Bader et al. and by Cremer et al. have related conjugative interactions to the existence of ellipticity (ε) in a bond, thus establishing a direct link with the molecular charge density—an observable property.[12] According to these studies, hyperconjugation is also reflected in the bond order n, which can be evaluated in terms of the charge density at the bond critical point (BCP), $\rho(\boldsymbol{r}_c)$.[12b] Accordingly, C–C bonds with $n > 1$ and $\varepsilon > 0$ can show evidence of hyperconjugative interactions. However, experimental evidence for charge transfer from a carbanion lone pair to an electronegative group, or of charge delocalization due to negative hyperconjugation, is still difficult to obtain. To observe such effects, analysis of atomic charges,[11] valence shell charge concentrations[13] and atomic dipole or quadrupole polarizations[14] offers charge-density-based criteria accessible by experiment.

Organolithium compounds have provided a challenge to chemical theories of structure and bonding since their discovery.[15] They share certain structural and chemical similarities with their transition metal counterparts. Thus, as early as 1950, β-hydride elimination in alkyllithium complexes was studied by Ziegler et al.[16] In 1974—a decade before the concept of agostic bonding was established—Stucky et al. reported close Li···H–C contacts in crystalline cyclohexyllithium.[17] In 1988 Kaufmann et al. introduced the term Li···H agostic interaction to account for this general phenomenon.[18] A recent Cambridge structural database search by Braga et al. revealed more than one hundred alkyllithium complexes with Li···H distances shorter than 2.20 Å.[19]

In this paper we apply theoretical and experimental methods to derive the charge-density distribution for a series of model organic and organolithium systems, and use Bader's AIM approach[11] to analyze this charge density in each case. We demonstrate that the charge concentrations in the valence shell of the α and β atoms of the alkyl fragment vary with the degree of electron delocalization from the α to the β atom. We also propose the concept of bond path ellipticity,[20,14b,21] as novel and general method to characterize the nature and extent of delocalization in alkyl complexes.

Results and Discussion

Charge distribution within the ethyl ligand: As this study explores the bonding in a series of ethyllithium complexes, we first consider the intrinsic charge distribution within the ethyl ligand and related organic moieties. We start with ethane, C_2H_6 (**1**): Figure 1a shows a relief map of the negative Laplacian of the charge density, $L(\boldsymbol{r}) = -\nabla^2\rho(\boldsymbol{r})$, for the electrons in one of the three symmetry-equivalent H-C-C-H planes at the B3LYP/6-311G(d,p) level of theory. Unless specified otherwise, this will be our standard level employed in the density functional theory (DFT) calculations. Positive

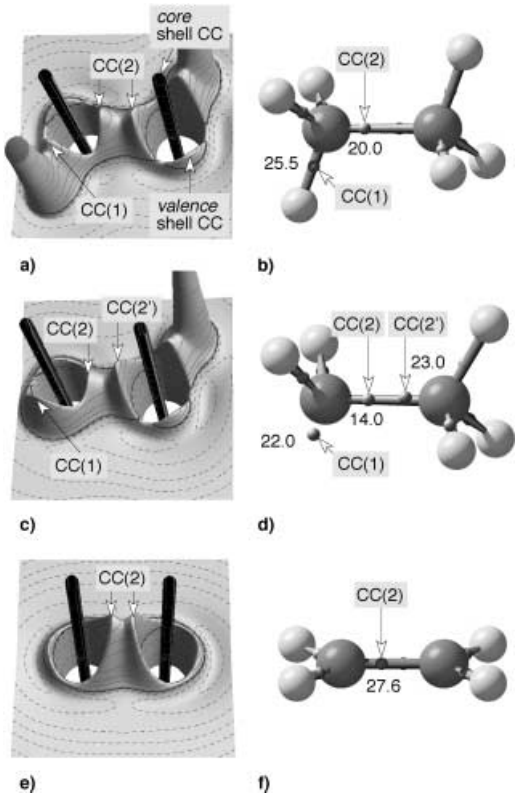

Figure 1. a), c), e): Relief map of the calculated negative Laplacian of the charge density, $L(\boldsymbol{r})$, in the C_α-C_β-H plane of ethane **1**, the ethyl anion **2**, and in the σ_v' plane (bisecting the CH_2 plane) of ethene **3**, respectively; default contour levels are drawn at -0.001, $\pm 2.0 \times 10^n$, $\pm 4.0 \times 10^n$, $\pm 8.0 \times 10^n$ e Å^{-5}, where $n = 0, 3, \pm 2, \pm 1$; positive and negative values are marked by solid and dashed lines, respectively. Extra contour lines at 15, 25, 84, 105, 240, 280, 350 e Å^{-5} are drawn, and the contour lines at 80, 200 and 400 have been omitted to reveal the relative positions of the CCs, which are indicated by arrows. b), d), f): Molecular representation of **1**–**3**, respectively, showing the spatial orientation of the CCs ($L(\boldsymbol{r})$ values are specified in e Å^{-5}).

values of the $L(\boldsymbol{r})$ function indicate that charge is locally concentrated at $\boldsymbol{r}$, whereas negative $L(\boldsymbol{r})$ values are characteristic of regions suffering local charge depletion. As shown by Bader et al.[12,22] the $L(\boldsymbol{r})$ function reveals the shell structure of the atoms. Accordingly, the principal quantum shells of the carbon atoms in ethane, K and L, are characterized by regions of charge concentration and depletion (Figure 1a). The charge concentration (CC) in the L shell of the carbon atoms, the so-called valence shell charge concentration (VSCC), appears to be rather distorted showing local maxima and minima. Indeed, the $L(\boldsymbol{r})$ functions in Figure 1a reveal two maxima in the L shell of each carbon atom in the H-C-C-H plane. These two maxima or $(3, -3)$ critical points[11] are henceforth denoted as bonded charge concentrations [bonded CC(1) and CC(2)], since they are located on the C–H and C–C bond paths.[23] In Figure 1a the relative positions of CC(1) and CC(2) are revealed by the contour lines at 25.5 and 20.0 e Å^{-5}, respectively. In total, four such maxima are evident, located along each of the three C–H bonds and the unique C–C bond; Figure 1b shows the relative location of all four CCs. In addition to their location, these four CCs can also be classified by their relative magnitudes. Thus, CC(2) for **1**, with a value of 20.0 e Å^{-5}, represents our benchmark value for the bonded CC for a symmetrical C–C single bond.

Turning to the carbanionic system $[C_2H_5]^-$ (**2**), significant asymmetry is now apparent in the charge density, $\rho(\boldsymbol{r})$, along the C–C bond, as revealed by the different magnitudes of CC(2) and CC(2′) (14.0 and 23.0 e Å^{-5}, respectively; Figure 1c, d). CC(1), which characterized a C–H bond in **1**, now represents a nonbonded CC ($L(\boldsymbol{r}) = 22.0$ e Å^{-5}). This serves as our standard for the CC of a free, non-coordinated carbanion lone pair. Our third benchmark system, C_2H_4 (**3**), characterizing a symmetrical C=C double bond, displays only three CCs at each carbon atom, each of which is located within the molecular plane (Figure 1e, f). Thus, the two different types of carbon atoms in **1** (sp^3-hybridized) and **3** (sp^2-hybridized) can be clearly distinguished through the topology of $L(\boldsymbol{r})$.

Henceforth, we use these characteristic features to explore the nature of β-substituted alkyl ligands and a series of ethyllithium complexes, and we show that the electronic nature of a wide range of such systems can be analyzed reliably by consideration of the features outlined above for **1**–**3**.

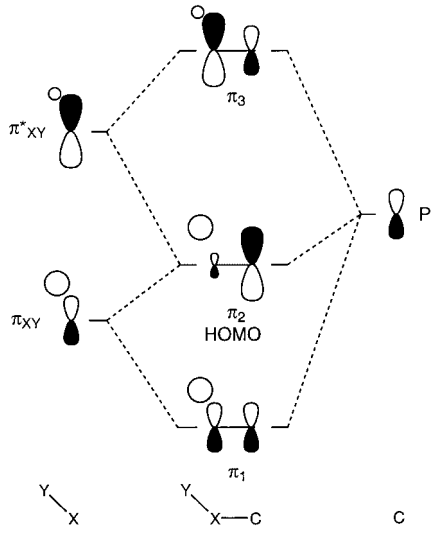

Scheme 1.

Stabilization of the ethyl ligand—negative hyperconjugation: We now address the stabilization of the alkyl ligand by negative hyperconjugation in alkyllithium complexes, and we show delocalization of the M–C bonding electrons to be the driving force behind this phenomenon.

In Figure 2 constant probability density surfaces of the HOMOs of C_2H_6 (**1**), $[C_2H_5]^-$ (**2**), and $[CH_2SiH_3]^-$ (**4**) are shown. The HOMO of C_2H_6 is C–C antibonding but C–H bonding.[24] The clear C–C antibonding character of the HOMO in ethane is less pronounced in the ethyl anion, while

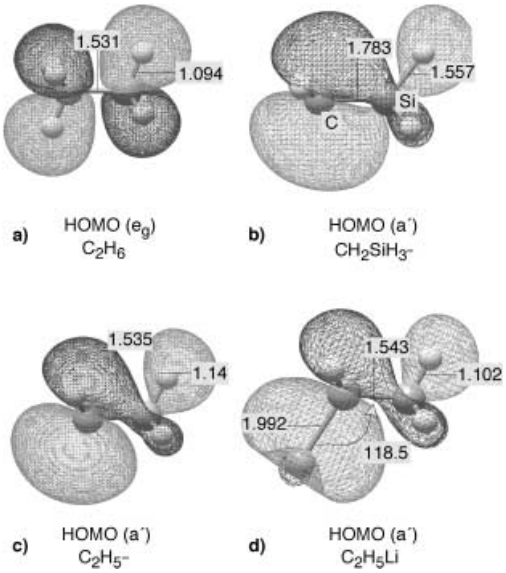

Figure 2. Constant probability density surfaces for the HOMOs of a) C_2H_6 (**1**), b) $CH_2SiH_3^-$ (**4**), c) $CH_2CH_3^-$ (**2**), and d) $LiCH_2CH_3$ (**5**).

in the case of our model system $CH_2SiH_3^-$, the HOMO already indicates a degree of π character in the C–Si bond. This can be interpreted as stabilization of the CH_2–SiH_3^- anion by negative hyperconjugation (Scheme 1).[8,25] According to the MO formulation of Schleyer et al. (Scheme 1), such negative hyperconjugation involves interaction of the occupied lone pair orbital (p) of the anion with the occupied π_{XY} and the vacant π^*_{XY} orbitals.[8]

In the case of the ethyl anion **2**, however, the $\pi^*_{CH} - p(C_\alpha)$ interaction is assumed to be weak, and the destabilising four electron $\pi_{CH} - p(C_\alpha)$ interaction dominates: thus the ethyl anion is assumed less stable than the methyl anion.[8] However, this situation is reversed when Y is an electronegative element. Here the $\pi^*_{XY} - p(C_\alpha)$ interaction is large and, in the extreme when Y = F, negative hyperconjugation forces complete transfer of charge to the fluoro ligand and a rupture of the C–F bond.[8] Thus, successful strategies developed to stabilize carbanions have generally relied on the introduction of second-row substituents at the α-position; these stabilize carbanions more efficiently than their first-row counterparts.[26] A silyl group is frequently employed in this respect, as this furnishes a polarizable and electropositive Si atom causing low-lying σ* orbitals which can support negative hyperconjugation.[26]

Figure 3a depicts the contour plot of $L(\boldsymbol{r})$ in the C_α-Si-H′ plane of $[CH_2SiH_3]^-$ (**4**), which suggests that the extent of negative hyperconjugation might be revealed quantitatively by the Laplacian of the total charge density of a molecule. Here we use the superscripts ′ or ″ to denote atoms located within or out of the plane of molecular symmetry, respectively. In fact, CC(1) ($L(\boldsymbol{r}) = 15.5$ e Å^{-5}) at the α-carbon atom appears significantly depleted compared with the corresponding CC in the ethyl anion (Figure 1c, d). This depletion of CC(1) in the lone pair region of the carbanion indicates a redistribution of charge within the valence shell of C_α, and may also signal charge delocalization over the C_α-Si-H′ moiety involved in negative hyperconjugation.[27]

The structural parameters deduced for **4** are consonant with such a description: the Si–H′ bond *anti* to the lone pair is clearly elongated (1.557 Å) and the C–Si bond is shortened (1.783 Å) compared with the corresponding values for CH_3SiH_3 **11** (1.488 and 1.885 Å, respectively).[28] The Si–H″ bonds (1.518 Å) are less affected, highlighting the dependence of the interaction between the π^*_{XY} orbital and the p carbanion orbital on the torsional angle (τ): hyperconjugation will be

  0947-6539/02/0810-2326 $ 20.00+.50/0 *Chem. Eur. J.* **2002**, *8*, No. 10

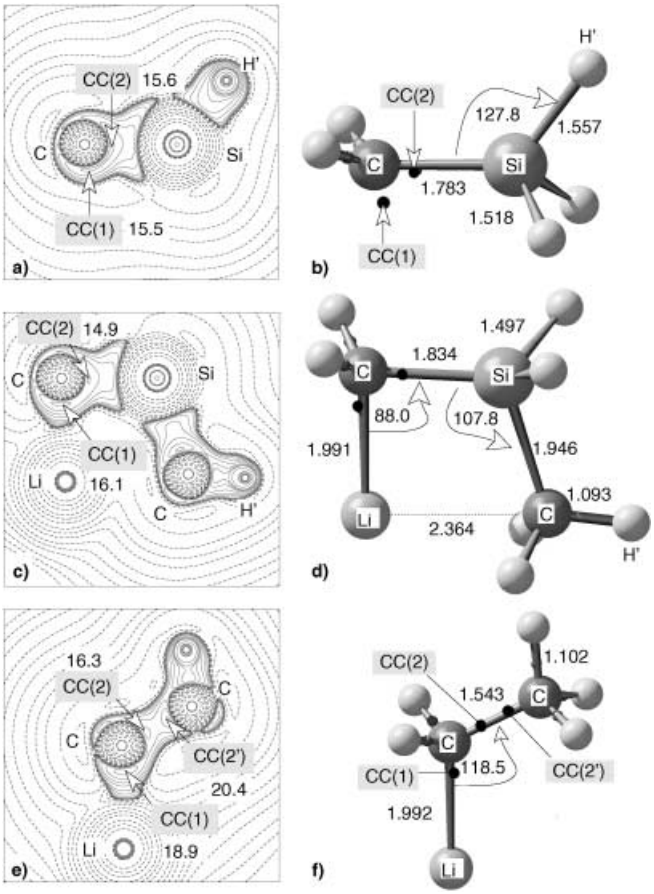

Figure 3. Contour maps of the calculated negative Laplacian of the charge density, $L(\boldsymbol{r})$, in the C_α-X_β-H′ plane (X = C, Si) of a) $CH_2SiH_3^-$ (**4**), c) $LiCH_2SiH_2CH_3$ (**6**), and e) $LiCH_2CH_3$ (**5**); default contour levels as specified in Figure 1 are drawn; solid lines correspond to positive values of $L(\boldsymbol{r})$ while broken lines indicate negative values of $L(\boldsymbol{r})$. b), d), f): Molecular representation of **4**–**6** showing the salient geometrical parameters (distances in Å; angles in °) and spatial orientation of the CCs ($L(\boldsymbol{r})$ values are specified in e Å^{-5}).

optimized at $\tau = 0$ and 180°, falling to zero at $\tau = 90°$.[8,29] The corresponding C–H′ bond in the ethyl anion is slightly enlarged by about 0.04 Å relative to the standard C–H bond in ethane **1**.[30]

Coordination of the ethyl ligand to lithium: We next consider how the charge distribution of the anion is perturbed by coordination to the lithium cation, the system $LiCH_2CH_3$ (**5**) representing the simplest such case. The significant asymmetry evident in the C–C bond of the ethyl anion **2** is redressed in **5**, with values for CC(2) and CC(2′) of 16.3 and 20.4 e Å^{-5}, respectively (Figure 3e, f). Furthermore, CC(1) ($L(\boldsymbol{r}) =$ 18.9 e Å^{-5}), which characterizes the anion lone pair in **2**, is significantly reduced in **5** on development of the Li–C bond, and shows a clear deformation towards the Li atom consonant with polarization of CC(1) by the highly Lewis acidic metal centre. The calculated Li–C bond length of 1.992 Å in **5** agrees well with that determined recently in the gas phase for $LiCH_3$ (1.959 Å).[31] The Li-C-C angle of 118.5° shows evidence of distortion at the α-carbon atom.[32,33] The topological features of $\rho(\boldsymbol{r})$ in **5** show the Li–C bond to be predominately ionic, with relatively depleted charge density at the BCP ($\rho(\boldsymbol{r}_c) =$ 0.150(2) e Å^{-3}), along with a negative value of $L(\boldsymbol{r}_c)$ (−4.90 e Å^{-5}). We note that values of $L(\boldsymbol{r}_c) > 0$ indicate that charge is locally concentrated at $\boldsymbol{r}_c$, while negative $L(\boldsymbol{r}_c)$ values are characteristic of regions suffering local charge depletion.[34] The energetic criteria[35] [$H(\boldsymbol{r}_c) = G(\boldsymbol{r}_c) + V(\boldsymbol{r}_c) =$ 0.007; $G(\boldsymbol{r}_c)/\rho(\boldsymbol{r}_c) = 1.17$] also point to an ionic Li–C bond,[36] while the reduced magnitude of CC(1) conforms with charge depletion of the lone pair at the α-carbon atom through polarization towards the metal centre.

At this stage it is pertinent to point out a further difference between the ethyl anion **2** and the lithium complex **5**. In **2** the C_β–H'_β bond was shown to be lengthened by about 0.04 Å, characteristic of weak hyperconjugative stabilization, whereas a normal C_β–H'_β bond (1.10 Å) and a slightly elongated C–C bond are calculated for **5** (Figure 3e, f), which represents the archetypal carbanion complex with no significant hyperconjugation. Here we need a new density-based criterion to discriminate clearly between hyperconjugation and charge polarization in the stabilization of carbanions. For this purpose we introduce the bond ellipticity ε as a measure of electron delocalization within an alkyl group. When ε is traced along the full C_α–X_β (X = C, Si) bond path, it serves as a very sensitive measure of distortion of the electron density from cylindrical, or σ symmetry.[12] According to the mathematical definition (Figure 4), ε values greater than zero indicate partial π character in a bond or electronic distortion away from σ symmetry along the bond path, as revealed by the ellipticity profile of the benchmark system ethene (**3**) along the C_α–C_β bond path.

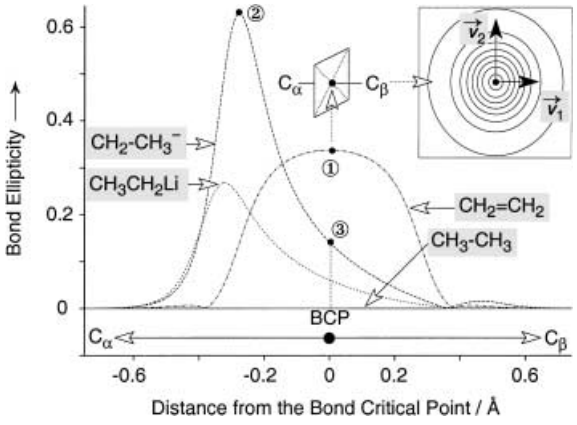

Figure 4. Calculated bond ellipticity profiles (ε) along the C_α–C_β bond path of $CH_2CH_3^-$ (**2**) and $LiCH_2CH_3$ (**5**) in comparison with C_2H_6 (**1**) and C_2H_4 (**3**). The definition of ε is illustrated by the $\rho(\boldsymbol{r})$ contour map in the right-hand corner showing the charge density in the plane perpendicular to the bond path at the C–C bond CP of **3** (denoted 1 in this figure). Thus, ε is a measure of the non-spherical charge distribution of $\rho(\boldsymbol{r})$: $\varepsilon = \lambda_1/\lambda_2 - 1$. λ_i are the eigenvalues of the corresponding eigenvectors $\boldsymbol{v}_1$ and $\boldsymbol{v}_2$ of the Hessian matrix of $\rho(\boldsymbol{r})$.

We note that **3** has a bell-shaped ellipticity profile around the BCP characteristic of a C=C double bond, whereas C_2H_6 (**1**) exhibits zero ellipticity along the whole bond path, indicating no deviation of $\rho(\boldsymbol{r})$ from σ symmetry. However, the situation is more complex for the carbanion systems $[CH_2CH_3]^-$ (**2**) and $LiCH_2CH_3$ (**5**). Despite different magni-

tudes of $\varepsilon(\boldsymbol{r})$, both **2** and **5** exhibit profiles characteristic of carbanionic C–C bonds, with a pronounced maximum in ε close to C_α and a non-zero value at the BCP. Analysis of the charge density in the plane perpendicular to the bond path at both ε_{max} and at the BCP of the C–C bond in **2** (Figure 5) reveals the different nature of ε at these salient points along the bond path.

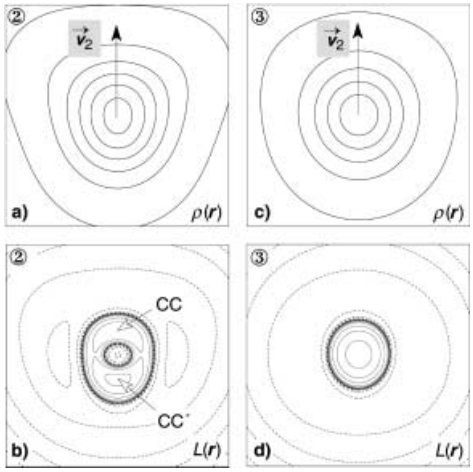

Figure 5. Contour maps of the calculated charge density, $\rho(\boldsymbol{r})$, and negative Laplacian of the charge density, $L(\boldsymbol{r})$, in the plane perpendicular to the bond path at both ε_{max} (denoted 2 in Figure 4), and at the BCP of the C–C bond in **2** (denoted 3 in Figure 4). The plane is oriented in each case such that the lone pair of **2** points down, whereas the C–H′ bond points up. The orientation of $\boldsymbol{v}_2$, the major axis of curvature, is indicated in a) and c) by an arrow. Default contour levels are drawn as specified in Figure 1. The two charge concentrations (CCs) around the C–C bond path at ε_{max} are labeled CC and CC′.

At ε_{max} the $\rho(\boldsymbol{r})$ contour map (Figure 5a) displays a pronounced asymmetry along the eigenvector $\boldsymbol{v}_2$ (major axis of curvature). In the positive direction the charge distribution appears more diffuse and deformed in the direction of the C_α–H bonds. This feature is clearly revealed by the corresponding $L(\boldsymbol{r})$ contour map in the same plane: two CCs of different magnitude (denoted CC and CC′ in Figure 5b) are evident. CC′ is more pronounced and is located close to CC(1), the CC in the lone pair region. Thus, the influence of CC(1) is still detectable along the C–C bond path close to the carbanionic carbon C_α. However, Figure 5c and 5d show that its influence on the charge distribution decreases significantly when the bond path approaches the BCP. Here the $\rho(\boldsymbol{r})$ and $L(\boldsymbol{r})$ contour maps indicate an elliptical charge distribution around the bond path, revealing some π-bonding character. Thus, the nature of charge distribution and the origins of charge deformation can be analyzed along the bond path. In this case, the smaller amount of negative hyperconjugation in **5** relative to **2** results in development of partial C=C character at the BCP, which is revealed in a unique manner by bond path analysis of $\varepsilon(\boldsymbol{r})$.

Li···H–C agostic interactions: The two preceeding sections describe how carbanions can be stabilized by negative hyperconjugation and/or coordination to Li^+, and how the charge-density distribution is altered by each of these processes. In this section we consider the existence of so-called Li···H–C agostic interactions and how these affect the charge distribution in the carbanion. Earlier, Kaufmann et al. considered the interaction in terms of $\sigma_{CH} \rightarrow$ Li donation of electron density,[18] by analogy with the model accepted at that time for agostic interactions in transition metal alkyls.[37]

In Figure 3c, d the model system $LiCH_2SiH_2Me$ (**6**) is shown. In accord with the experimental structures of Li[HC-$(SiHMe_2)_2$] (**7**)[38] and [{2-$(Me_3Si)_2CLiC_5H_4N$}$_2$] (**8**),[21,39] an acute Li-C-Si angle of 88.0° and short Li···H contacts of 2.258 Å are found for **6**.[40] Li···H contacts in the range 1.8–2.2 Å are typically considered to represent agostic interactions (for a general structural and statistical study on Li agostic systems see reference [19]). According to this definition, such interactions are clearly absent in $LiCH_2CH_3$ (**5**), but might be present in **6**. In this respect, **6** serves as perhaps the simplest model system for a complex displaying intramolecular agostic Li···H contacts. Figure 3c depicts the contour plot of $L(\boldsymbol{r})$ in the Li-C_α-Si plane of **6**. In comparison with **5** (Figure 3e), the CC in the lone pair region of the carbanion, denoted CC(1) (16.1 e Å^{-5}), is depleted yet further, as is CC(2) (14.9 e Å^{-5}); this is suggestive of redistribution of charge density by electron delocalization. Indeed, the structure shows two different C–Si bond lengths (C_α–Si = 1.834; Si–C_γ = 1.946 Å). A similar situation pertains for the related carbanion $[CH_2SiH_2Me]^-$ (**6a**) (C_α–Si = 1.773; Si–C_γ = 1.953 Å), implying the presence of negative hyperconjugation in **6**. However, the conformation of the alkyl backbone in **6** is radically different from that in **6a**. In the anion **6a** the position of the methyl group is energetically favored in an *anti* orientation towards CC(1), and the C-Si-C angle (125.4°) is widened by more than 17° relative to **6**.[41] So why is the orientation of the terminal methyl group reversed and accompanied by an acute Li-C-Si angle in the lithium complex **6** and the experimental structures of **7** and **8**? Clearly, negative hyperconjugation is not the only phenomenon exerting an influence on the electronic structure of **6**. Are additional Li···H–C interactions the driving force for the geometrical deformations of the alkyl ligand?

The answer to this question is provided by a combined high-resolution X-ray and neutron diffraction charge-density study on [{2-$(Me_3Si)_2CLiC_5H_4N$}$_2$] (**8**) at 115 K and a further low temperature neutron diffraction study at 20 K.[21] We first discuss the geometry of **8** on the basis of the neutron measurement and in the next step its electronic structure derived from the combined charge density study. Figure 6 shows the relevant molecular fragment in **8** on the basis of the neutron study at 20 K. An acute Li-C1-Si2 angle of 88.8(2)° results in short Li···Si2, Li···C7, and Li···H7c contacts of 2.850(5), 2.658(5), and 2.320(6) Å, respectively. In addition, two further short intermolecular Li···H contacts (Li···H3b* = 2.329(5) and Li···H3c* = 2.245(5) Å) and a rather short Li···C3* contact of 2.496(4) Å are evident. All the Li···H contacts are remarkably short (ca. 0.7 Å less than the sum of the van der Waals radii; cf. the Li···H distance of 2.043(1) in crystalline LiH),[42] suggestive of agostic Li···H interactions. However, no significant elongation of the C–H bonds is evident from the neutron diffraction data (C7–H7a = 1.089(4), C7–H7b = 1.086(4), C7–H7c = 1.087(4) Å;

  0947-6539/02/0810-2328 $ 20.00+.50/0 *Chem. Eur. J.* **2002**, *8*, No. 10

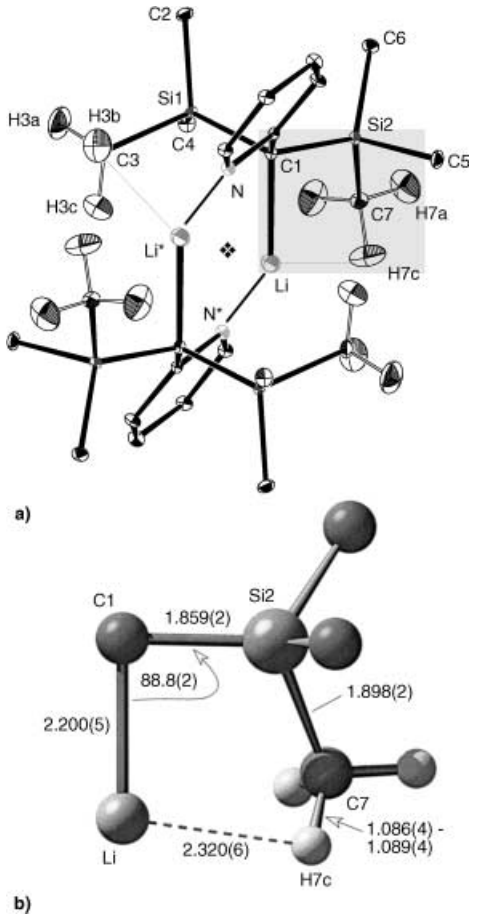

Figure 6. Molecular structure of $[\{2\text{-}(Me_3Si)_2CliC_5H_4N\}_2]$ (**8**) based on a single crystal neutron diffraction study at 20 K; probability level 50 %. Only relevant H atoms are shown. Atoms labeled with or without * are related by a crystallographic inversion center at the midpoint of the Li–Li* vector. a) The location of the agostic alkyl group is indicated by a shaded area. b) The corresponding agostic alkyl backbone is shown and salient geometrical parameters are given; distances in Å and angles in °.

C3–H3b = 1.085(3), C3–H3c = 1.097(4) Å). The same is true for the B3LYP/6-31G(d) optimized geometry of **8** and also for the calculated model systems **6**, **7**, and $LiCMe_2SiMe_3$ (**9**). In spite of short Li···H–C contacts in all computed model systems (**6**: 2.258 Å; **7**: 2.170–2.348 Å; **9**: 2.106-2.308 Å), no corresponding C–H bond elongation characteristic of agostic interaction was observed (**6**: 1.104 Å; **7**: 1.100-1.104 Å; **9**: 1.101-1.105 Å; C–H bond lengths corresponding to short Li···H–C contacts < 2.4 Å; for comparison, see C–H bond lengths in the terminal methyl group of **5**: 1.097–1.102).[43,44,45] Thus, agostic Li···H–C interactions do not appear to be the driving force responsible for the unusual geometry of **8**. Inspection of the total charge density within the Li-C1-Si2 plane (Figure 7a) indeed reveals no significant charge accumulation between H7c and Li. In contrast to the Li–C1 bond, no BCP exists for the Li···H contact. As pointed out in a combined experimental and theoretical charge density study the existence of a M···H–C bond critical point is not a necessary condition for the presence of an agostic interaction.[45b] However, the absence of any charge accumulation between Li and H_γ rules out significant covalent interaction.[46] The same is true for the intermolecular Li···H3c contact. However, in this case an *inter*molecular Li···C3 BCP is found in both the experimental and the calculated total charge density ($\rho(\boldsymbol{r}_c) = 0.082(1)$ [0.06] e Å^{-3}; $L(\boldsymbol{r}) = -0.828(1)$ [1.30] e Å^{-5}; $\varepsilon = 0.69$ [0.98]; calculated values in square brackets).

Thus, Li···H–C interactions are not pronounced in **6** and **8**; the deformation of the alkyl skeletons in **6** and **8** seems to result instead from delocalization of the Li–C_α bonding electrons over the *entire* alkyl group, resulting in a reduced Li-C_α-Si_β angle, pronounced C_α–Si_β double bond character, short Li···Si_β, Li···C_γ, and Li···H_γ distances, and thus facilitating more efficient charge transfer between the electron-deficient metal centre and the agostic C_α-Si_β-C_γ-H_γ backbone (C_α, Si_β, C_γ, and H_γ correspond to C1, Si2, C7, and H7c in **8**, respectively).[21] Indeed, both **6** and **8** show low calculated $L(\boldsymbol{r})$ values for CC(1) (16.1 and 13.5 e Å^{-5}), and CC(2) (14.9 and 15.0 e Å^{-5}), respectively. In Figure 7b the corresponding experimental $L(\boldsymbol{r})$ contour map is shown. There is a pronounced difference in magnitude between CC(1) and CC(2) (18.0 and 24.6 e Å^{-5}, respectively), and, in addition, the experimental $L(\boldsymbol{r})$ values for **8** are in general larger than the corresponding calculated ones.[47] However, the general trend—delocalization of the carbanionic lone pair—is consistently revealed by both experiment and theory. Figure 7c shows an envelope map as an alternative representation of the experimental $L(\boldsymbol{r})$ function at C1. In this representation, the close-to-merging situation between the two valence charge concentrations CC(1) and CC(2) is clearly visible and indicates delocalization of the Li–C bonding electrons.

The conclusion that delocalization, rather than Li···H–C agostic interaction, is responsible for the observed distortions

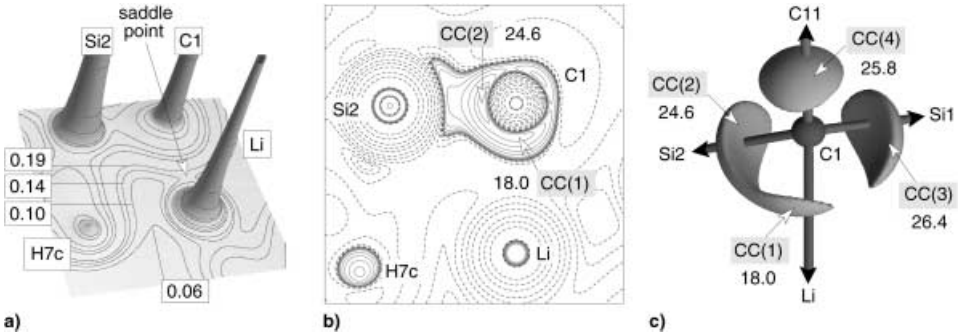

Figure 7. a) Total experimental charge density, $\rho(\boldsymbol{r})$, inside the Li,C1,Si2 plane of $[\{2\text{-}(Me_3Si)_2CLiC_5H_4N\}_2]$ (**8**). Default contour levels are drawn at 0.06, 0.1, 0.142, 0.19, 0.4, 0.54, 0.8, 1.45, 1.85, 4, 8, 20 e Å^{-3}. The saddle point, or (3, –1) BCP between C1 and Li is indicated by an arrow and allocated between the contour lines at 0.14 and 0.19 e Å^{-3}. b) Contour map of the experimental $L(\boldsymbol{r})$ function in the Li,C1,Si2 plane of **8**. Default contour levels as specified in Figure 1 are drawn; solid lines correspond to positive values of $L(\boldsymbol{r})$, while broken lines indicate negative values of $L(\boldsymbol{r})$. The valence charge concentrations denoted CC(1) and CC(2) almost merge into each other. c) This close-to-merging situation of CC(1) and CC(2) is more clearly revealed at C1 by an envelope map of $L(\boldsymbol{r})$ at 17 e Å^{-5}.

is further supported by the bond ellipticity profiles of [{2-$(Me_3Si)_2CLiC_5H_4N\}_2$] (**8**) and of the model systems $[CH_2SiH_3]^-$ (**4**) and $CH_2{=}SiH_2$ (**10**) (Figure 8).[48] Complex **8** represents the first system for which calculated and experimental $\varepsilon(\boldsymbol{r})$ plots have been compared. These profiles show

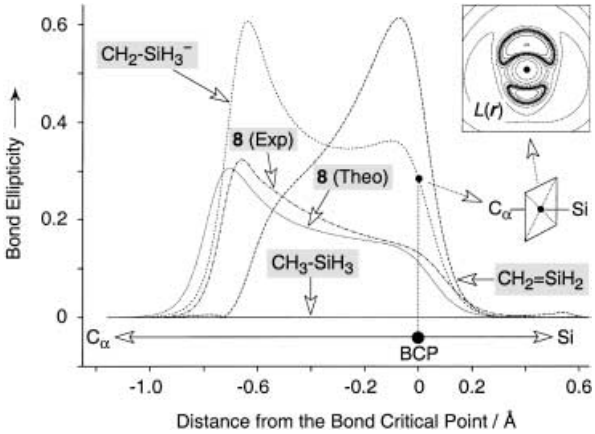

Figure 8. Experimental and calculated bond ellipticity profiles (ε) along the C_α-Si_β bond path of **8** (C_α and Si_β correspond to C1 and Si2, respectively) in comparison with $CH_2SiH_3^-$ (**4**), CH_2SiH_2 (**10**), and CH_3SiH_3 (**11**). In the right-hand corner the corresponding $L(\boldsymbol{r})$ function at the BCP of **4** is shown, revealing that charge is locally concentrated above and below the molecular plane of **4** resulting from the presence of π-electron density.

remarkable agreement. However, the bond profile is rather complex, showing a pronounced maximum in $\varepsilon(\boldsymbol{r})$ close to C_α and a shoulder close to the BCP. This maximum highlights once again the influence of the carbanion lone pair on the charge distribution in the region of C_α. The shoulder can, however, be related to C=Si double bond character as revealed in the model system $CH_2{=}SiH_2$ **10**. Compound **8** clearly shows a pronounced degree of C=Si character, whereas the carbanion nature is reduced in comparison with $[CH_2SiH_3]^-$ (**4**).

The C_α=Si double bond character in **8** is also revealed by the geometrical and topological features at the BCPs obtained by a topological analysis of the experimental charge density. The Li-C_α-Si_β-C_γ-H_γ backbone displays two significantly different C–Si bonds: C_α–Si_β and C_γ–Si_β (C1–Si2 = 1.8592(4) and Si2–C7 = 1.8947(7) Å). Whereas C_γ–Si_β is slightly enlarged compared with a standard single C–Si bond such as Si2–C5(6) or Si1–C2(4) (Si–C = 1.8781(7) – 1.8888(6) Å), C_α–Si_β is clearly shortened. Furthermore, the discrepancy in Si–C bond lengths is accompanied by significant differences in the nature of the C_α–Si and C_γ–Si bonding. The value of $\rho(\boldsymbol{r})$ at the BCP, $\rho(\boldsymbol{r}_c)$, for the C_α–Si_β bond ($\rho(\boldsymbol{r}_c) = 0.86(2)$ e Å^{-3}) is clearly larger than that for the corresponding C_γ–Si_β bond (0.72(2) e Å^{-3}), implying a greater bond order in the C_α–Si than in the C_γ–Si bond.

Hence, we conclude that charge polarization along the Li–C_α bond, delocalization of the Li–C_α bonding electrons, and additional electrostatic interactions between the C_α-Si_β-C_γ-H_γ backbone and the metal centre all play a role in stabilizing **8**.

Conclusion

The charge distribution within the ethyl anion $[C_2H_5]^-$ (**2**) and the related organic moieties C_2H_6 (**1**) and C_2H_4 (**3**) has been explored by DFT calculations, and the valence shell charge concentrations thus deduced have been charted, revealing characteristic features of the bonding and electronic structure of these species. Replacement of the C_β atom by Si in **2** leads to significant delocalization of the lone pair charge density on C_α through negative hyperconjugation. This is clearly revealed by a depletion of the lone pair charge concentration CC(1). This delocalization is also revealed in the geometry of $[CH_2SiH_3]^-$ (**4**), with a shortening of the C_α–Si bond and elongation of the Si–H bond *anti* to the lone pair. When **2** is coordinated to Li^+ to produce LiC_2H_5 (**5**), the lone pair is strongly polarized towards the metal, resulting in a predominantly ionic Li–C bond with an Li-C-C angle of 118.5° and a normal C–H bond distance *anti* to the Li–C bond; this precludes significant hyperconjugative or Li···H–C agostic interactions. The anion $[CH_2SiH_2Me]^-$ (**6a**) displays significant asymmetry in its Si–C bond lengths, with Si–C_α approximately 0.2 Å shorter than Si–C_γ, and a terminal methyl group *trans* to the anionic lone pair. In its lithium complex, $LiCH_2SiH_2Me$ (**6**), the asymmetry in the Si–C bond lengths is preserved, but the conformation is quite different to **6a**, with a smaller C_α-Si-C_γ angle, an acute Li-C-Si angle, and the terminal methyl group *cis* to the anionic lone pair, resulting in a short Li···H–C_γ contact. These features result from a combination of 1) negative hyperconjugative delocalization of the Li–C_α bonding electrons along the alkyl fragment and 2) additional secondary interactions as signaled by the short Li···Si, Li···C_γ, and Li···H_γ contacts. These additional secondary interactions appear to be reponsible for the energetic preference of the *cis* orientation of the terminal methyl group to the Li–C bond.

The conclusions drawn for these calculated systems are corroborated by an experimental X-ray and neutron diffraction charge-density study[21] on [{2-$(Me_3Si)_2CLiC_5H_4N\}_2$] (**8**), which shows similar distortions in its Li-C_α-Si_β-C_γ-H_γ fragment. Here also, there is neither significant elongation apparent for the C_γ–H bonds, nor any evidence of significant agostic Li···H–C interactions. Electron delocalization and stabilization by additional secondary interactions between the metal and the alkyl backbone allow distortion of the ligand by drawing the Si_β-C_γ-H_γ fragment towards the metal. The delocalization of the Li–C electron density is revealed by an envelope of the Laplacian of the charge density, which clearly shows a significant depletion of CC(1), the charge concentration in the region of the carbanionic lone pair at the C_α atom. Furthermore, both valence shell charge concentrations CC(1) and CC(2) (located in the Li-C_α-Si plane) appear to merge into each other, suggesting a partial rehybridization from sp^3 towards sp^2 at the C_α atom. Thus, the carbanion character in **8** is reduced by negative hyperconjugation, a conclusion supported by the geometry and the topology of the electron density of **8**, which both imply significant double bond character for the C_α–Si bond and a bond order $n < 1$ for the Si–C_γ bond.

Bond ellipticity (ε) profiles have been calculated for most of the model systems presented, and have been used to reveal

  0947-6539/02/0810-2330 $ 20.00+.50/0 *Chem. Eur. J.* **2002**, *8*, No. 10

the nature and extent of electron delocalization in each case, with good agreement between experimental and calculated profiles. The asymmetry in ε charts the degree of π character (or deviation from σ symmetry) along a bond path, whereas the position and magnitude of ε_{max} reveals the extent of delocalization of the lone pair in a carbanion.

Charge concentrations and bond ellipticity profiles have each been shown to be reliable and sensitive criteria for quantifying the extent of electron delocalization in the model systems presented here. Both parameters can be derived from the charge density; hence, they are physical observables, which are accessible both by experiment and theory. Although the application of these novel criteria is limited in this study to simple organic and organolithium species, these simple but powerful concepts are applicable across a wide range of chemical and bonding situations, including organo-transition metal complexes, and inorganic or organometallic rings and clusters.[49] Hence, they offer the first direct experimental measure of delocalization, and open up exciting possibilities for the exploration of this phenomenon in all its guises.

Experimental Section

Neutron diffraction of 8: A well-formed, yellow crystal with dimensions $4.5 \times 2.2 \times 1.7$ mm was fixed and sealed under nitrogen atmosphere in a suitable glass capillary for neutron data collection. Three-dimensional data were collected using the hot neutron four-circle diffractometer D9 (100 K measurement) and the thermal neutron four-circle diffractometer D19 (20 K measurement) at the ILL reactor (Institut Laue-Langevin, Grenoble, France), equipped with a two-stage Displex cryorefrigerator and a $8^\circ \times 8^\circ$ ($64^\circ \times 4^\circ$) position sensitive detector. Values for the measurement on D19 are given in parentheses. A Cu (220) monochromator in reflection geometry was used to select a neutron beam of wavelength 0.82306 Å (0.9507 Å). The sample was slowly cooled (2 K min^{-1}) to 100 K (20 K), while monitoring a strong reflection. No splitting or change in mosaicity of the peak was observed.

Intensity data [100 K: $h(-18/18)$, $k(0/15)$, $l(-15/15)$, $2\theta_{max} = 79.9^\circ$; 20 K: $h(-13/13)$, $k(-5/11)$, $l(-5/14)$, $2\theta_{max} = 67.6^\circ$] were measured by means of coupled ω-$x\theta$ scans with a scan width between 1.5 and 2.9° and x ranging from 0 to 1.8 (20 K: ω-scans, scan width between 1.8 and 2.4°). The initial measuring time of about 2.5 s per step (21 000 monitor counts per step, 31 steps) was increased to approximately 4.2 s (35 000 monitor counts per point) for higher angle data. In the D19 experiment the measuring time was 4.1 s per step (48 000 monitor counts per step, 31 steps). During the whole measurement three strong reflections were monitored regularly and showed no significant variation. In addition, two Ψ scans indicated that absorption and extinction effects should be negligibly small ($\mu_{eff} = 2.31$ cm^{-1}). No significant $\lambda/2$ component was observed.

In all, 4322 (4077) reflections were collected and integrated in three dimensions by using the ILL program "Racer" ("Retreat"). The final unit cell [100 K: $a = 11.7220(13)$, $b = 9.8640(12)$, $c = 12.7517(15)$ Å, $\beta = 93.479(4)^\circ$, $\alpha = \gamma = 90^\circ$; 20 K: $a = 11.6982(5)$, $b = 9.8218(5)$, $c = 12.6895(6)$ Å, $\beta = 93.5114(19)^\circ$] was determined by the ILL program "Rafd9" ("Rafd19"). After merging with the program "SHELXL-97",[50] a sum of 3811 (2161) independent reflections remained ($R_{int} = 0.0216$ and 0.0407, respectively) which were used for a full-matrix least-squares refinement (in the monoclinic space group $P2_1/n$) by minimizing $\Sigma w(F_o^2 - F_c^2)^2$ with a "SHELXL-97" weighting scheme. The initial atomic coordinates for the heavy atoms were taken from the X-ray structure determination and the neutron scattering lengths were taken to be $b_c(C) = 6.646$, $b_c(H) = -3.739$, $b_c(Li) = -1.90$, $b_c(N) = 9.36$, and $b_c(Si) = 4.1491$ fm.[51] During the refinement, difference Fourier maps clearly revealed all of the hydrogen atom positions: all atoms of the asymmetric unit were refined anisotropically, giving a final R value of 0.0330 (R_1 [$I > 2\sigma(I)$]; 20 K: 0.0311) and 0.0670 (wR_2 [$I > 2\sigma(I)$]; 20 K: 0.0652), respectively (GOF = 1.083 and 1.098, respectively; shift/err < 0.001).

X-ray diffraction study of 8

Data collection: A well-formed, yellow crystal with the dimensions $1.12 \times 0.41 \times 0.28$ mm was glued inside a 0.01 mm thin-walled capillary and mounted on a Nonius KappaCCD detector system. The sample was cooled with an Oxford Cryostream System to 115 K in 1.5 h with a mean temperature gradient of -2 K min^{-1}. Preliminary examination and final data collection were carried out with graphite-monochromated $Mo_{K\alpha}$ radiation ($\lambda = 0.71073$ Å) generated from a Nonius FR 591 rotating anode running at 50 kV and 60 mA. Intensity data were collected using 1° ϕ and ω scans with a detector-to-sample distance of 40 mm. For the low-order data ten scan sets (1257 frames in total) were collected at a scan angle (Θ) in the range of 0.0 to -17.0° and a scan time between 5 and 30 seconds per frame. For the high-order data four scan sets (455 frames in total; $\Theta = -32^\circ$) with a scan time of 120 seconds per frame were chosen.[52]

Data reduction: Crystal data for [{2-$(Me_3Si)_2CLiC_5H_4N$}$_2$] at 115 K: $M_r = 486.85$, $a = 11.7233(2)$, $b = 9.8814(2)$, $c = 12.7702(2)$ Å, $\beta = 93.4810(11)^\circ$, $V = 1476.60(5)$ Å^3; monoclinic; space group $P2_1/n$; $Z = 2$; $F(000) = 528$; $\rho_{calcd} = 1.095$ g cm^{-3}; $\mu = 0.22$ mm^{-1}. The unit cell was determined from 28 093 reflection positions. An initial orientation matrix was determined from ten frames of the first scan set and refined during the integration of the individual scan sets. The intensities were first corrected for beam inhomogeneity and crystal decay by the program "Scalepack" using a tight scale restraint (0.001).[52b] An absorption correction was then applied ($T_{min} = 0.795$, $T_{max} = 0.942$) and symmetry equivalent and multiply measured reflections were averaged with the program "Sortav".[53] After rejection of 2025 statistically out-lying reflections, the internal agreement factor was $R_{int}(I) = 0.0360$ for a total of 78 323 reflections yielding 15 534 unique reflections. This data set provided 97.5 % of data in $5.4 < 2\Theta < 101.2^\circ$ ($\sin\Theta/\lambda < 1.087$ Å^{-1}).

Multipolar refinements and determination of the deformation density: First, an independent atom model (IAM) refinement was carried out, in which all atoms were treated as spherical. Anisotropic thermal parameters were introduced to describe the thermal motion of all non-hydrogen atoms. All hydrogen atoms were found in the difference map and refined isotropically. The refinement finally converged at $R_1 = 0.061$, $wR_2 = 0.104$ and $GOF = 1.089$ for 12 231 reflections ($\sin\Theta/\lambda < 1.00$ Å^{-1}) and 233 parameters.[50]

A multipole model was then adopted to describe the deformation of $\rho(\boldsymbol{r})$ from a spherical distribution. According to a method proposed by Stewart,[54] the electron density $\rho(\boldsymbol{r})$ in a crystal is described by a sum of aspherical pseudoatoms at the nuclear positions $\{\boldsymbol{R}_j\}$ [Eq. (1)].

$$\rho(\boldsymbol{r}) = \sum_j \rho_j(\boldsymbol{r} - \boldsymbol{R}_j) \tag{1}$$

Based on the Hansen–Coppens formalism,[55] the pseudoatom density $\rho_j(\boldsymbol{r} - \boldsymbol{R}_j)$ is expressed in terms of multipoles [Eq. (2)]:[56]

$$\rho_j(\boldsymbol{r}_j) = P_c\rho_c(r_j) + \kappa'^3 P_v\rho_v(\kappa' r_j) + \sum_{l=0}^{l_{max}} \sum_{m=-l_{max}}^{+l_{max}} \kappa''^3 P_{lm} R_l(\kappa'' r_j) Y_{lm}(\theta_j, \phi_j) \tag{2}$$

In the refinement of our best model the multipole expansion was truncated at the octapole level ($l_{max} = 3$) for the heavy atoms carbon, nitrogen, and silicon. Lithium and hydrogen were treated with monopoles ($l = 0$) and, in the case of hydrogen, with bond-directed dipoles ($l = 1$) in addition. Core and spherical valence densities were constructed using Clementi and Roetti Hartree–Fock (HF)[57] atomic wave functions expanded over Slater-type basis functions.[58] The radial functions for the valence deformation densities were of single Slater-type. During the refinement the Li and H atom positions were fixed at the values obtained by neutron diffraction (100 K), while their anisotropic displacement parameters were scaled by the average ratio ($U_{ij,\ X\text{-}ray}/U_{ij,\ neutron}$) = 1.30 to account for the temperature difference. The thermal parameters of the heavy atoms were freely refined. To reduce the number of multipole populations to be refined the two methyl group carbons C2, C4 and C5, C6, respectively, the aromatic carbons C12, C13, and C14, the aromatic hydrogens (H12, H13, H14, H15) and all methyl group hydrogens, except for H3b, H3c, H7b and H7c, were assumed to be chemically equivalent (chemically constrained model, see also S3, S4 in the Supporting Information). In addition, local C_3 pseudosymmetry was imposed on C2, C4, C5, and C6, and a local pseudo

mirror plane on C12, C13, C14, and C15. A radial scaling (κ') for the spherical density was refined for each heavy atom type while for H atoms κ' was kept fixed (1.20). In addition, for chemically non-equivalent atoms different κ' factors were used (14 in total). The molecule was kept neutral during all refinements.

With the experimental model this procedure refined to $\kappa' = 1.051(7)$ and 1.031(7) for Si2 and Si1, respectively, $\kappa' = 0.983(2)$ for N, $\kappa' = 0.966$(fixed) for C1, $\kappa' = 0.986(3)$ for C2 and C4, $\kappa' = 0.984$(fixed) for C3, $\kappa' = 0.984(3)$ for C5 and C6, $\kappa' = 0.985(5)$ for C7, $\kappa' = 1.030(4)$ for C11, and $\kappa' = 1.009(2)$ for C12, C13, C14, and C15. Both fixed κ' values were obtained by refinement, but fixed in the last cycle due to correlation. The final agreement factors were $R_1 = 0.0250$, $wR_2 = 0.0314$, and $GOF = 1.062$ for 8905 reflections ($F_o > 3\sigma(F_o)$; $\sin\Theta/\lambda < 1.00\,\text{Å}^{-1}$) and 301 parameters ($N_{ref}/N_{var} = 29$). The residual electron density map was practically featureless with the maximum and minimum values of 0.21 and -0.20 e Å^{-3} ($\sin\Theta/\lambda < 0.8\,\text{Å}^{-1}$), respectively (see also S5b in the Supporting Information for details).

Hirshfeld's rigid bond test[59] was applied to the atomic displacement parameters obtained from the refinements. The difference between mean-square amplitudes for all heavy atom bonds except for the Si–C bonds Si2–C6, Si2–C7, Si1–C2, Si1–C3, and Si1–C4 is within the limit of $1.0 \cdot 10^{-3}$ Å^2 proposed by Hirshfeld. However, the difference for the above-mentioned Si–C bonds, due to the different masses of the bonded atoms, is somehow larger, but never exceeds a value of $1.8 \cdot 10^{-3}$ Å^2.[60] CCDC-169890, CCDC-169891, and CCDC-169892 contain the supplementary crystallographic data for this paper. These data can be obtained free of charge via www.ccdc.cam.ac.uk/conts/retrieving.html (or from the Cambridge Crystallographic Data Centre, 12 Union Road, Cambridge CB21EZ, UK; fax: (+44) 1223-336-033; or e-mail: deposit@ccdc.cam.ac.uk).

Computational details: All refinements were carried out with the full-matrix least-squares program "XDLSM" of the "XD" suite of programs;[56] the quantity minimized was $\varepsilon = \Sigma w_1(|F_o| - k|F_c|)^2$, where k is a scale factor, based on 8905 reflections with $F_o > 3\sigma(F_o)$. Weights were taken as $w_1 = 1/\sigma^2(F_o)$. Convergence was assumed when a maximal shift/esd $< 10^{-11}$ was achieved. For the topological analysis, critical points of the electron density were searched by a Newton Raphson algorithm implemented in "XD". Properties of $\rho(\boldsymbol{r})$ and $\nabla^2\rho(\boldsymbol{r})$ were calculated after transformation of the local axis system into a global system.[61]

DFT calculations with the Becke3LYP density functional[62] were carried out with the "Gaussian98" program suite.[63] Unless specified otherwise, the 6–311G(d,p)[64] basis set was our standard for all model systems. Only compound **8** was optimized employing the 6–31G(d) basis set, while the topological analysis was performed at the B3LYP/6–311G(d,p)//B3LYP/6–31G(d) level of theory. All geometry optimizations of our model systems [except **1** (D_{3d}), **2** (C_s), **3** (D_{2h}), **4** (C_s), **5** (C_s), **6a** (C_s), **6** (C_s), **7** (C_s), **10** (C_{2v}), **11** (C_{3v})] were performed without imposing any symmetry constraints; see also the Supporting Information and references [30, 38, 40, 41] for further information. All models were found to be minima on the potential energy surface by calculating analytical frequencies. The topological analysis of the theoretical electron densities was carried out with the "AIMPAC" software package.[65]

Acknowledgements

This work was supported by the Deutsche Forschungsgemeinschaft and the Fonds der Chemischen Industrie. We gratefully thank Prof. W. A. Herrmann for his support, the Alexander von Humboldt Foundation for a Postdoctoral Fellowship (to D.S.), and for support through an Australian Research Council Large Grants Scheme (M.G.G.).

[1] a) E. Hückel, *Z. Phys.* **1931**, *70*, 204–286; b) E. Hückel, *Z. Phys.* **1931**, *72*, 310–337; c) E. Hückel, *Z. Physik* **1932**, *76*, 628–648.
[2] a) L. Pauling, *Proc. Natl. Acad. Sci. USA* **1932**, *18*, 293–297; b) L. Pauling, J. Sherman, *J. Chem. Phys.* **1933**, *1*, 606–617.
[3] L. Pauling, G. W. Wheland, *J. Chem. Phys.* **1933**, *1*, 362–374.
[4] G. W. Wheland, *Resonance in Organic Chemistry*, Wiley, New York, **1955**.
[5] R. S. Mulliken, *J. Chem. Phys.* **1933**, *1*, 492–503.
[6] J. D. Roberts, R. L. Webb, E. A. McElhil, *J. Am. Chem. Soc.* **1950**, *72*, 408–411.
[7] a) E. L. Eliel, *Angew. Chem.* **1972**, *84*, 779–791; *Angew. Chem. Int. Ed. Engl.* **1972**, *11*, 739–750; b) E. L. Eliel, S. H. Wilen, *Stereochemistry of Organic Compounds*, Wiley, New York, **1994**.
[8] P. von R. Schleyer, A. J. Kos, *Tetrahedron*, **1983**, *39*, 1141–1150.
[9] "Origin and Quantitative Modeling of Anomeric Effect": P. Petillo, L. Lerner, *ACS Symp. Ser.* **1993**, *539*, 156–175.
[10] a) F. Weinhold, *Nature* **2001**, *411*, 539–541; b) V. Pophristic, L. Gooman, *Nature* **2001**, *411*, 565–568.
[11] "Atoms in Molecules: A Quantum Theory": R. F. W. Bader, *Int. Ser. Monogr. Chem.* **1994**, *22*, 1–438.
[12] a) R. F. W. Bader, T. S. Slee, D. Cremer, E. Kraka, *J. Am. Chem. Soc.* **1983**, *105*, 5061–5068; b) D. Cremer, E. Kraka, T. S. Slee, R. F. W. Bader, C. D. H. Lau, T. T. Nguyen-Dang, P. J. MacDougall, *J. Am. Chem. Soc.* **1983**, *105*, 5069–5075.
[13] S. T. Howard, J. P. Foreman, P. G. Edwards, *Inorg. Chem.* **1996**, *35*, 5805–5812.
[14] See for example: a) C. Heinemann, T. Müller, Y. Apeloig, H. Schwarz, *J. Am. Chem. Soc.* **1996**, *118*, 2023–2038; b) M. Tafipolsky, W. Scherer, K. Öfele, G. Artus, W. A. Herrmann, G. S. McGrady, *J. Am. Chem. Soc.* **2002**, in press.
[15] See, for example: a) W. N. Setzer, P. von R. Schleyer, *Adv. Organomet. Chem.* **1985**, *24*, 353–451; b) A. B. Sannigrahi, T. Kar, B. Guha-Niyogi, P. Hobza, P. von R. Schleyer, *Chem. Rev.* **1990**, *90*, 1061–1076.
[16] K. Ziegler, H. G. Gellert, *Justus Liebigs Ann. Chem.* **1950**, *567*, 179–184.
[17] R. Zerger, W. Rhine, G. Stucky, *J. Am. Chem. Soc.* **1974**, *96*, 6048–6055.
[18] E. Kaufmann, K. Raghavachari, A. E. Reed, P. von R. Schleyer, *Organometallics* **1988**, *7*, 1597–1607.
[19] D. Braga, F. Grepioni, K. Biradha, G. R. Desiraju, *J. Chem. Soc. Dalton Trans.* **1996**, 3925–3930.
[20] a) J. R. Cheeseman, M. T. Carroll, R. F. W. Bader, *Chem. Phys. Lett.* **1988**, *143*, 450–458; b) F. Cargnoni, C. Gatti, *Theor. Chem. Acc.* **2001**, *105*, 309–322; c) F. Cargnoni, C. Gatti, L. Colombo, *Phys. Rev. B.* **1998**, *57*, 170–177.
[21] W. Scherer, P. Sirsch, M. Grosche, M. Spiegler, S. A. Mason, M. G. Gardiner, *Chem. Commun.* **2001**, 2072–2073.
[22] a) R. F. W. Bader, H. Essén, *J. Chem. Phys.* **1984**, *80*, 1943–1960; b) R. P. Sagar, A. C. T. Ku, V. Smith, *J. Chem. Phys.* **1988**, *88*, 4367–4374; c) Z. Shi, R. J. Boyd, *J. Chem. Phys.* **1988**, *88*, 4375–4377.
[23] For a definition of the bond path or atomic interaction line which follows the ridge of the charge density between bonded atoms see reference [11].
[24] Hence, this is termed the π_z^* orbital of ethane or the ethyl ligand.
[25] P. von R. Schleyer, T. Clark, A. J. Kos, G. W. Spitznagel, C. Rhode, D. Arad, K. N. Houk, N. G. Rondan, *J. Am. Chem. Soc.* **1984**, *106*, 6467–6475.
[26] See for example: a) A. E. Reed, P. von R. Schleyer, *J. Am. Chem. Soc.* **1990**, *112*, 1434–1445; b) A. E. Reed, C. Schade, P. von R. Schleyer, P. V. Kamath, J. Chandrasekar, *J. Chem. Soc. Chem. Commun.* **1988**, 67–69.
[27] Although negative hyperconjugation is defined as an orbital interaction, charge transfer as well as polarization may be a consequence of delocalization; see reference [8].
[28] Similar values have been obtained earlier (ref. [25]). For consistency, the anionic model systems in this work are discussed on the basis of our standard basis set, even though diffuse basis sets should be used for an adequate description of carbanionic systems. However, neither the topological features nor the geometry changes significantly when more diffuse and flexible basis sets are employed (see Supporting Information for results employing various basis set combinations).
[29] See for example: a) G. Gundersen, D. W. H. Rankin, H. E. Robertson, *J. Chem. Soc. Dalton Trans.* **1985**, 191–197; b) G. Gundersen, R. A. Mayo, D. W. A. Rankin, *Acta Chem. Scand. Ser. A* **1984**, *38*, 579–591; c) D. G. Anderson, A. J. Blake, S. Cradock, E. A. V. Ebsworth, D. W. H. Rankin, A. J. Welch, *Angew. Chem.* **1986**, *98*, 97–99; *Angew. Chem. Int. Ed. Engl.* **1986**, *25*, 107–108.
[30] However, the C–C bond in the ethyl anion is rather invariant compared with ethane, as a consequence of the weak π^*_{CH}-p(C_α)

  0947-6539/02/0810-2332 $ 20.00+.50/0 *Chem. Eur. J.* **2002**, *8*, No. 10

interaction in **2** (Figure 2, Scheme 1). Thus, negative hyperconjugation is not predominant in **2** in contrast to **4**. However, we note, that **2** is the only system in our study that shows a strong dependency of the geometrical and charge density parameters on the choice of the basis set. Thus, at the B3LYP/6–311++G(3df,3pd) level of theory the C–C bond in **2** is shorter than the one in **1** at the same level of theory (1.525 vs. 1.531 Å) and CC(1) in **2** becomes rather depleted (17.0 e Å^{-5}). Thus, the effect of negative hyperconjugation is present in the ethyl anion but is revealed only when rather diffuse and flexible basis sets are employed.

[31] D. B. Grotjahn, T. C. Pesch, J. Xin, L. M. Ziurys, *J. Am. Chem. Soc.* **1997**, *119*, 12368–12369.

[32] As noted before (see for example R. Boese, D. Bläser, N. Niederprüm, M. Nüss, W. A. Brett, P. von R. Schleyer, M. Bühl, N. J. R. v. Eikema Hommes, *Angew. Chem.* **1992**, *104*, 356–358; *Angew. Chem. Int. Ed. Engl.* **1992**, *31*, 314–316) the C-C-X angles are wider for electropositive X substituents: these induce larger C-C-X angles in the pyramidalized carbanions on account of the more pronounced carbanion character at the C_α atom. Similar wide M-C-C angles can be also observed in early transition metal complexes such as $EtTiCl_3$ (Ti-C-C = 116.6(11)°); see ref. [33] for further information.

[33] W. Scherer, T. Priermeier, A. Haaland, H. V. Volden, G. S. McGrady, A. J. Downs, R. Boese, D. Bläser, *Organometallics* **1998**, *17*, 4406–4412.

[34] $L(\boldsymbol{r}_c)$ at a (3,1) bond CP describes the nature of the interaction between bonded atoms as ionic ($L(\boldsymbol{r}_c) < 0$) or covalent ($L(\boldsymbol{r}_c) > 0$). $L(\boldsymbol{r}_c)$ is related to the principal curvatures λ_i ($i = 1, 2, 3$) of $\rho(\boldsymbol{r}_c)$; λ_3 is the curvature along the bond path and is always positive, while λ_1 and λ_2 are the curvatures perpendicular to the bond path and are always negative. If $|\lambda_1| + |\lambda_2| > \lambda_3$, a positive value of $L(\boldsymbol{r}_c)$ results, indicating a contraction of the charge density towards the bond path and thus implying the presence of a covalent bond.

[35] Cremer and Kraka pointed out that analysis of $L(\boldsymbol{r}_c)$ gives a rather sensitive measure of the charge-density accumulation, but is not always sufficient to distinguish between covalent and closed-shell interactions. The chemical bonding can be described sufficiently only when both the electron-density based criteria and energetic contributions are taken into account. They therefore proposed analysis of the electronic kinetic energy density $G(\boldsymbol{r})$ and the electronic potential energy density $V(\boldsymbol{r})$ at the bond critical point, since the magnitudes of both are related to the Laplacian by an equation derived by Bader (R. F. W. Bader, *J. Chem. Phys.* **1980**, *73*, 2871–2883) viz. $2G(\boldsymbol{r}) + V(\boldsymbol{r}) = 1/4\nabla^2\rho(\boldsymbol{r})$. For covalent bonds it has been shown that the local energy density $H(\boldsymbol{r}_c) = G(\boldsymbol{r}_c) + V(\boldsymbol{r}_c)$ is less than zero (D. Cremer, E. Kraka, *Angew. Chem.* **1984**, *96*, 612–614; *Angew. Chem. Int. Ed. Engl.* **1984**, *23*, 627–628), and that, in addition, the ratio $G(\boldsymbol{r}_c)/\rho(\boldsymbol{r}_c)$ should be less than unity (P. Macchi, D. M. Proserpio, A. Sironi, *J. Am. Chem. Soc.* **1998**, *120*, 13429–13435).

[36] The nature of the Li–C bond is the subject of controversy in the literature. On the basis of a natural population analysis monomeric $LiCH_3$ is reported to be 88% ionic (ref. [18]), whereas the degree of ionicity of the Li–C bond (50%) was asssumed not to dominate when Hirshfeld charges are taken into account (F. M. Bickelhaupt, N. J. R. van Eikema Hommes, C. F. Guerra, E. J. Baerends, *Organometallics* **1996**, *15*, 2923–2931).

[37] M. Brookhart, M. L. H. Green, L.-L. Wong, *Prog. Inorg. Chem.* **1988**, *36*, 1–124.

[38] a) J. L. Atwood, T. Fjeldberg, M. F. Lappert, N. T. Luong-Thi, R. Shakir, A. J. Thorne, *J. Chem. Soc. Chem. Commun.* **1984**, 1163–1165; b) T. Fjeldberg, M. F. Lappert, A. J. Thorne, *J. Mol. Struct.* **1985**, *127*, 95–105; c) We note in contrast to the polymeric solid state structure (Li-C-Si = 87.7–103.1°), a non-acute Li-C-Si angle of 115(2)° was found by gas electron diffraction (GED; see ref. [38b] for a detailed description). However, B3LYP/6–311G(d,p) calculations starting at the experimental geometry of the GED study converged to a C_s symmetric structure with two Li-C-Si angles of 87.4°, in good agreement with the solid-state structure. Frequency calculations confirmed this geometry as a minimum on the potential energy surface (Li–C = 1.998, C_α–Si = 1.829, Si–C_γ = 1.950, Li···$H1_\gamma$ = 2.170, Li···$H2_\gamma$ = 2.348, Li···$H3_\gamma$ = 3.428, C_γ–$H1_\gamma$ = 1.104, C_γ–$H3_\gamma$ = 1.094 Å; $\tau(LiC_\alpha SiC_\gamma) = -7.2°$). We note that the experimental difficulties inherent in locating the light Li atom in the presence of a bulky ligand containing two heavy Si atoms may be responsible for the discrepancies observed between the calculated, solid-state, and gas phase structures deduced for this benchmark compound.

[39] R. I. Papasergio, C. L. Raston, A. H. White, *J. Chem. Soc. Chem. Commun.* **1983**, 1419–1420.

[40] We report all structural and topological parameters of **6** based on geometry opimizations implying C_s symmetry constraints. Frequency calculations indicate that the C_s geometry might represent a first-order transition state at the B3LYP/6-311G(d,p) level (one imaginary frequency; 33*i*). However, refinements without any symmetry constraints reveal only insignificant changes in geometry away from C_s symmetry. Since also the total energy remains virtually unchanged (< 0.01 kcal mol^{-1}) we report only data for the C_s model. We further note, that the energy for **6** assuming an all-staggered C_s conformation with a fixed Li-C-Si angle of 112° is only 0.62 kcal mol^{-1} higher in energy. Thus, the Li-C-Si potential-energy surface appears to be rather featureless.

[41] Even under the constraints of C_s symmetry, the hypothetical *cis* conformer of **6a** is unstable with respect to inversion at C_α and is energetically disfavored, while the 180° form, in which the Si–CH_3 bond and the carbanion lone pair interact through hyperconjugation, is most stable. The energetic preference of the 180° form over the 0° form has been been discussed in detail for other benchmark compounds in the literature; e.g. refs. [8, 25].

[42] E. Zintl, A. Harder, *Z. Phys. Chem. Abt. B* **1935**, *28*, 478–480.

[43] According to the classical definition of agostic C–H bonds given by Brookhart, Green, and Wong, the agostic C–H distance falls in the range 1.13–1.19 Å, and is elongated 5–10% relative to a nonbridging C–H bond (ref. [37]). Indeed, strong agostic Li···H–C interactions have been observed and confirmed experimentally by neutron diffraction only for CD_2Li_2 (ref. [44]). In this case, short Li···D(2)–C distances of 2.06(2) Å, and correspondingly a significantly elongated C–D(2) bond of 1.18(2) Å were observed; furthermore the shortest known Li···H distance of 1.72(3) (Li···D(1)–C) is also established for this compound. For typical agostic C–H bond lengths in early transition metal complexes see for example ref. [45].

[44] a) G. D. Stucky, M. M. Eddy, W. H. Harrison, R. Lagow, D. E. Cox, *J. Am. Chem. Soc.* **1990**, *112*, 2425–2427; b) J. J. Novoa, M.–H. Whangbo, G. D. Stucky, *J. Org. Chem.* **1991**, *56*, 3181–3183.

[45] a) A. Haaland, W. Scherer, K. Ruud, G. S. McGrady, A. J. Downs, O. Swang, *J. Am. Chem. Soc.* **1998**, *120*, 3762–3772; b) W. Scherer, W. Hieringer, M. Spiegler, P. Sirsch, G. S. McGrady, A. J. Downs, A. Haaland, B. Pedersen, *Chem. Commun.* **1998**, 2471–2472; c) D. C. McKean, G. S. McGrady, A. J. Downs, W. Scherer, A. Haaland, *Phys. Chem. Chem. Phys.* **2001**, *3*, 2781–2794.

[46] In the case of strong agostic interactions, however, M···H BCPs are observed with $\rho(\boldsymbol{r}_c)$ values in the typical range of hydridic M–H bonds (> 0.5 e Å^{-3}); W. Scherer, M. Tafipolsky, P. Sirsch, unpublished results.

[47] Further combined experimental and theoretical topological studies of the $L(\boldsymbol{r})$ function are needed to evaluate the origin of this small discrepancy. However, the $L(\boldsymbol{r})$ function—as the negative Laplacian of the charge density—is of course very sensitive to small changes in the charge density distribution. Thus, the agreement between theory and experiment is surprisingly good.

[48] We note that the smaller CC in **10** (see $L(\boldsymbol{r})$ contour map in the right-hand corner of Figure 8) is directed inwards in the agostic cyclic fragment (Li, C_α, Si_β, C_γ, H_γ), as expected for a cyclic delocalized system (ref. [12a]).

[49] W. Scherer, P. Sirsch, G. S. McGrady, E. Gullo, unpublished results.

[50] G. M. Sheldrick, SHELXL-97, Program for Crystal Structure Refinement, University of Göttingen, Germany, **1997**.

[51] V. F. Sears, *Neutron News* **1992**, *3*, 26–37.

[52] a) COLLECT Data Collection Software, Nonius B.V., **1998**; b) "Processing of X-ray Diffraction Data Collected in Oscillation Mode": Z. Otwinowski, W. Minor, *Methods Enzymol.* **1997**, *276*, 307–326.

[53] R. H. Blessing, *Acta Crystallogr. A* **1995**, *51*, 33–38.

[54] R. F. Stewart, *Acta Crystallogr. A* **1976**, *32*, 565–574.

[55] H. K. Hansen, P. Coppens, *Acta Crystallogr. A* **1978**, *34*, 909–921.

[56] T. Koritsanszky, S. T. Howard, Z. Su, P. R. Mallinson, T. Richter, N. K. Hansen, XD, Computer Program Package for Multipole Refinement and Analysis of Electron Densities from Diffraction Data, Free University of Berlin, Germany, **1997**.

[57] E. Clementi, C. Roetti, *At. Data Nucl. Data Tables* **1974**, *14*, 177 – 478.
[58] E. Clementi, D. Raimondi, *J. Chem. Phys.* **1963**, *38*, 2686 – 2689.
[59] F. Hirshfeld, *Acta Crystallogr. A* **1976**, *32*, 239 – 244.
[60] a) J. D. Dunitz, V. Schomaker, K. N. Trueblood, *J. Phys. Chem.* **1988**, *92*, 856 – 867; b) J. D. Dunitz, E. F. Maverick, K. N. Trueblood, *Angew. Chem.* **1988**, *100*, 910 – 926; *Angew. Chem. Int. Ed. Engl.* **1988**, *27*, 880 – 895.
[61] The search for critical points in the negative Laplacian of the experimental charge density, $L(\boldsymbol{r})$, was performed with the help of the Newton – Raphson method implemented in the XDPROP program by Dr. M. Tafipolsky. The same algorithm is used in the BUBBLE program (written by P. Krug, **1990**) of the AIMPAC suite of programs (ref. [65]).
[62] a) A. D. Becke, *J. Chem. Phys.* **1993**, *98*, 5648 – 5652; b) C. Lee, W. Yang, R. G. Parr, *Phys. Rev. B* **1988**, *37*, 785 – 789.
[63] GAUSSIAN 98, Revision A.7, M. J. Frisch, G. W. Trucks, H. B. Schlegel, G. E. Scuseria, M. A. Robb, J. R. Cheeseman, V. G. Zakrzewski, J. A. Montgomery, Jr., R. E. Stratmann, J. C. Burant, S. Dapprich, J. M. Millam, A. D. Daniels, K. N. Kudin, M. C. Strain, O. Farkas, J. Tomasi, V. Barone, M. Cossi, R. Cammi, B. Mennucci, C. Pomelli, C. Adamo, S. Clifford, J. Ochterski, G. A. Petersson, P. Y. Ayala, Q. Cui, K. Morokuma, D. K. Malick, A. D. Rabuck, K. Raghavachari, J. B. Foresman, J. Cioslowski, J. V. Ortiz, B. B. Stefanov, G. Liu, A. Liashenko, P. Piskorz, I. Komaromi, R. Gomperts, R. L. Martin, D. J. Fox, T. Keith, M. A. Al-Laham, C. Y. Peng, A. Nanayakkara, C. Gonzalez, M. Challacombe, P. M. W. Gill, B. Johnson, W. Chen, M. W. Wong, J. L. Andres, C. Gonzalez, M. Head-Gordon, E. S. Replogle, and J. A. Pople, Gaussian, Inc., Pittsburgh PA, USA, **1998**.
[64] a) A. D. McLean, G. S. Chandler, *J. Chem. Phys.* **1980**, *72*, 5639 – 5648; b) R. Krishnan, J. S. Binkley, R. Seeger, J. A. Pople, *J. Chem. Phys.* **1980**, *72*, 650 – 654.
[65] F. W. Biegler-König, R. F. W. Bader, T. Tang, *J. Comput. Chem.* **1982**, *3*, 317 – 328.

Received: October 29, 2001 [F3639]

  0947-6539/02/0810-2334 $ 20.00+.50/0